

Experimental investigation of organic fouling mitigation in membrane filtration and removal by magnetic iron oxide particles

Jaehyun Jung^b, Mark Sibag^c, Bora Shin^d and Jinwoo Cho^{*}

Department of Environment and Energy, Sejong University, Seoul 05006, Korea

(Received November 10, 2019, Revised January 17, 2020, Accepted February 20, 2020)

Abstract. Here magnetic iron oxide particles (MIOPs) were synthesized under atmospheric air and which size was controlled by regulating the flow rate of alkali addition and used for efficient removal of bovine serum albumin (BSA) from water. The MIOPs were characterized using field-emission scanning electron microscopy (FE-SEM), Fourier transformation-Infrared spectroscopy (FT-IR) and vibrating sample magnetometer (VSM). The results revealed a successful preparation of the MIOPs. The removal efficiency for BSA using MIOPs was found to be about 100% at lower concentrations (≥ 10 mg/L). The maximum adsorption of 64.7 mg/g for BSA was achieved as per the Langmuir adsorption model. In addition, microfiltration membrane for removal of BSA as model protein organic foulant is also studied. The effect of various MIOPs adsorbent sizes of 210, 680 and 1130 nm on the absorption capacity of BSA was investigated. Water permeability of the BSA integrated with the smallest size MIOPs membrane was increased by approximately 22% compared by the neat BSA membrane during dead-end filtration. Furthermore, the presence of small size MIOPs were also effective in increasing the permeate flux.

Keywords: magnetic iron oxide particles; organic fouling; membrane bioreactor; organic fouling

1. Introduction

Contamination of water with natural organic matters (NOMs) is one of the most serious dilemma faced the global community due to their highly risk effect on human health (Esmat *et al.* 2017). The bovine serum albumin (BSA) is one of these NOMs. Currently, numerous common techniques have been extensively employed for BSA removal from wastewater, including adsorption, precipitation, membrane filtration and ion exchange (Guo *et al.* 2015, Huang and Keller 2015, Maher *et al.* 2014). The efficient adsorption technique for the removal of BSA has various advantages over the other techniques such as economical, simple and used for numerous years (Gavrilescu 2004, J. Wang and Chen 2009). Recently, applying of nanomaterials in the adsorption and environmental applications has received a considerable interest due to their high surface area and greater adsorption capacity (Abbas *et al.* 2018, Tawfik *et al.* 2017). Various adsorbents such as titanate nanotubes, Fe-Al binary oxide, alginate biopolymer and their composites were used to remove the BSA (Hao *et al.* 2010, Kim and Jang, 2018, Lakouraj *et al.* 2014, Tu *et al.* 2013, Zhang *et al.* 2010). However, Magnetic iron oxide particles (MIOPs) are a well-known adsorbent that can be found naturally and synthesized. They are widespread in nature as minerals containing Fe in divalent (ferrous) and/or trivalent (ferric) state and O in rocks, sediments and soils. Under favorable conditions, they exhibit significant sorptive interaction with

many different compounds, including fractions of NOMs in environmental systems (Adegoke, Adekola, Fatoki and Ximba, 2013). They can be synthesized in the laboratory under experimentally controlled conditions for tailored applications such as carriers of biomolecules (Chen *et al.* 2015, Mehta, 2017). The inherent adsorption capability of MIOPs and their magnetic property are of a special interest in both scientific and technological research for potential applications in wastewater treatment. MIOPs could significantly reduce the amount of the BSA component of NOM in wastewater, which is one the many reported contributing factors of organic fouling in membrane bioreactors (MBR) (Lee, Amy and Lozier, 2005, H. Wang *et al.* 2017). Thus, MIOPs could facilitate mitigation of organic fouling and offer a more convenient way of separating them from activated sludge. However, this application of MIOPs is still in the experimental and developmental stage (Gutierrez, Dziubla and Hilt, 2017, Xu *et al.* 2012). The application of magnetic iron oxide in MBR would require that the size of magnetic iron oxide particles is less than that of the membrane pore size (Semblante *et al.* 2013). A simple way to control the size of magnetic iron oxides is to control the flow rate of alkali addition during synthesis (Gnanaprakash, Philip, Jayakumar and Raj, 2007). Magnetic iron oxides can be synthesized in many ways depending on the desired characteristics. For wastewater treatment in MBR, the co-precipitation method would be a cost-effective choice (Khalil 2015, Li and Sui 2012, Mascolo, Pei and Ring 2013). Drying of magnetic iron oxide particles in air atmosphere also does not compromise its intended use as magnetic adsorbents (Karaagac, Kockar, Beyaz and Tanrisever 2010). Although recently the potential of magnetic iron oxide particles for the mitigation of

*Corresponding author, Professor
E-mail: jinwoocho@sejong.edu

membrane fouling has been demonstrated there is still a limited number of studies on this research area. In this paper, we present the results of our investigation of MIOPs and the removal of BSA as a model proteinaceous organic foulant. We discuss how MIOPs could mitigate membrane fouling in the context of dead-end filtration. The interaction between MIOPs and BSA results in the mitigation of membrane fouling was also explained.

2. Materials and methods

2.1 Synthesis of magnetic iron oxide particles

Simple co-precipitation method was used to synthesis the magnetic iron oxide particles (MIOPs). The iron salts, such as (0.8 M) FeCl₃·6H₂O and (0.4M) FeSO₄·7H₂O were acidified with 35% hydrochloric acid (HCl) and sulfuric acid (H₂SO₄), respectively. An equal volume of the two acidified solutions were mixed (1:1). The resulting mixture was placed in a heating mantle under vigorous mixing and left until 70°C temperature was attained. Five different sets of experiment were performed to check the effect of alkali addition rate on nanoparticle synthesis by adding sodium hydroxide at different flowrates (1ml/min, 2.5ml/min, 5ml/min, 10 ml/min and 15 ml/min). For every flowrate alkali was added until pH 9 was attained. After each set of experiment pH was slowly adjusted to pH 5 with the addition of HCl to precipitate out the iron from the mixture. A magnetic force was applied to separate this precipitated iron from the mixture and it was rinsed with the DI water (3 times at 60°C) to remove ionic impurities trapped or adhered to the particle coagulum and set to the oven for drying at 45°C. Thereafter, nanoparticles were soaked in nitric acid (HNO₃) for about 3 hours and again they were rinsed with DI water (3 times at 60°C). These MIOPs were finally dispersed in ethanol and stored for further characterization and subsequent application in batch experiments.

2.2 Characterization techniques for MIOPs

All samples were inspected by field-emission scanning electron microscopy (FE-SEM) using HITACHI S-4700 instrument. The images were then obtained to investigate the morphology of the nanoparticles. The saturation magnetization was obtained using a superconducting quantum interference device (S700X SQUID Magnetometer, Cryogenic Limited, UK) in the applied magnetic field range of -10,000 Oe to 10,000 Oe. The hydrodynamic size and zeta potential of the nanoparticles were measured at 25 °C by dynamic light scattering (DLS) and electrophoretic light scattering (ELS), respectively (PSS Nicomp, Sta. Barbara, CA, USA). Vibrational spectroscopy studies were used Fourier-transform infrared (FTIR), attenuated total reflectance (ATR) analysis, (Spectrum 100, Perkin Elmer, USA). The spectrum was obtained in the wavelength range of 650 to 4000 cm⁻¹. The capacity of the removal of nanoparticles was studied using UV-Vis spectrophotometer (Shimadzu-UV-1800).

2.3 Batch kinetics and adsorption experiments

Bath adsorption experiments were conducted by adding the magnetite iron oxide with 2.5 mg/L concentration to all different concentration of Bovine Serum Albumin (BSA) protein. Total volume of each glass vial was 10 ml. The vials were agitated at speed (285 rpm) in rotary shaker for 24 hours. After that, the magnetite iron oxide was separated from the test solution by magnet for around 1 hour. Then the prepared sample solutions were passed through to the adsorption measurement with the UV absorption method. We have used 1 ml quartz cuvette for all samples. All experiments were carried out at ambient temperature (25±2 °C).

The Langmuir isotherm equation can be expressed as:

$$\frac{C_e}{q_e} = \frac{C_e}{q_0} + \frac{1}{q_0 K_L} \quad (1)$$

where:

C_e : the concentrations of BSA in the solution at equilibrium (mg/L)

q_e : the amount of BSA adsorbed on magnetite at equilibrium (mg/g)

q_0 : the maximum amount of BSA adsorbed on MIOPs(mg/g)

K_L : the Langmuir adsorption constant (ml/mg)

q_0 and K_L are calculated from the slope and intercept of the linear plot of C_e/q_e versus C_e .

It should be noted that C_e and q_e are obtained experimentally based on the following equation:

$$q_e = \frac{C_0 - C_e}{m} V \quad (2)$$

where:

C_e : the concentrations of BSA in the solution at equilibrium (mg/L)

C_0 : the initial concentration of BSA (mg/L)

q_e : the amount of BSA adsorbed on magnetite at equilibrium (mg/g)

m : the mass of MIOPs (g)

The Freundlich isotherm can be expressed as following equation:

$$q_e = K_f C_e^{1/n} \quad (3)$$

where, K_f and $1/n$ are the Freundlich constant characteristics of the system, indicating the adsorption capacity and adsorption intensity, respectively. Equation can be linearized in logarithmic form:

$$\ln q_e = \ln K_f + 1/n \ln C_e \quad (4)$$

Pseudo first and second order equations were fitted to the dataset to observe the kinetics changes on the adsorption of BSA on MIOPs.

The First order equation can be expressed as:

$$q_t = q_e(1 - e^{-k_t t}) \quad (5)$$

where, q_t and q_e are the adsorbed solute amount after adsorption at the time point t and the equilibrium time, respectively. k_t (1/h) represents the pseudo first model constant and t is adsorption time.

Table 1 Membrane specifications

Characteristics	Durapore® membrane
Material	Hydrophobic polyvinylidene fluoride
Pore size	0.22 μm
Wettability	Hydrophobic
Thickness	125 μm
Air flow rate	16 L/min \times cm ²
Porosity	75%
Water flow rate	>1 L/min \times cm ²
Filter surface	plain

The pseudo second order equation can be expressed as:

$$\frac{t}{q_t} = \frac{1}{k_2 q_e^2} + \frac{1}{q_e} \quad (6)$$

where, q_t is the adsorbed amount of adsorbate at any time t and q_e is the amount of adsorbate adsorbed at equilibrium condition.

2.4 Membrane

Dead-end filtration was conducted to determine the filtration resistance of the BSA solution after contact with MIOPs. A microfiltration membrane disc was used. Cut a 31.7 cm² disc from a roll of a flat-sheet PVDF membrane. The specifications of the membrane were listed in Table 1. Membrane has been soaked in a methanol solution for 1 min to facilitate membrane wetting and rinse with DI water. Immediately proceed to the next step before the membrane disc filter dries up. Perform membrane pre-compaction (L. Wang *et al.* 2013), so that the membrane would not be compacted nor swelled during the dead-end filtration test. This is to ensure that the overall change in permeate flux during the test is mainly due to membrane fouling (L. Wang *et al.* 2013).

2.5 Dead-end filtration experiment

Place the membrane in the test cell then pour the sample into the test cell. Push the cap assembly down onto the cell body, using a twisting motion and orienting the inlet port on the opposite the permeate port on the holder. Set the pressure relief valve know to the horizontal (open) position. Slide the cell into the retaining stand, fitting the ring on the cell base into the hole in the stand.

Place a receiving container above an electronic balance. Fill the feed reservoir with the desired volume of sample and close the lid. Turn on the nitrogen gas valve and slowly regulate the pressure up to 30 kPa. Monitor the weight of the permeate with time. Open the WinCT software, which allows real-time monitoring of the data retrieve from the electronic balance.

Place the receiving container above the electronic balance. Tare the electronic balance. Perform membrane pre-compaction for 30 minutes (L. Wang *et al.* 2013) although it may be extended for long hours (e.g up to 50 h) depending on the membrane materials.

The total resistance, R_T , of a virgin membrane with DI water is its membrane resistance, R_m . The imposed feed pressure is increased incrementally by 10 kPa every ten minutes starting from 5 kPa to 20 kPa. The desired values of imposed pressure can be set by manually adjusting the pressure regulator upstream of the feed reservoir. Switch on the electronic balance, wait for a stable reading, put a receiving container on top and press tare.

Turn on the WinCT software. Set the pressure regulator to 5 kPa and monitor the changes in permeate volume for ten minutes. Incrementally increase the pressure by 5 kPa every ten minutes starting from 5 kPa up to 25 kPa. Monitor the changes in permeate volume during the ten-minute test period. Determine the equivalent volumetric flow rate for each applied feed pressure from the slope of the increase in permeate volume over time. The corresponding permeate flux is calculated based on the equation:

$$\text{Volumetric flow rate} = \text{flux} \times \text{filter area} \quad (9)$$

where flux in liter/m²/h and filter area in m².

From the plot of TMP versus permeate flux, calculate the membrane resistance based on the equation:

$$R = \frac{\text{TMP}}{\mu J} \quad (10)$$

where:

R is the Initial membrane resistance, 1/m, TMP is the Transmembrane pressure, kPa, μ is the Viscosity, Ns/m² and J is the Permeate flux, L/m²/h.

3. Result and discussion

3.1 MIOPs synthesis and characterizations

MIOPs samples with different sizes were separately diluted in deionized (DI) water and dispersing by sonication for 10 min in a bath-type sonicator at room temperature (25 C°). The dispersal samples were filtered using a 0.2 μm filter using vacuum filtration. Finally, the samples for using in FE-SEM measurement would be dried at room temperature. Figure 1 shows the morphology of low to high particle size of MIOPs which characterized by hydrothermal process. It is clear that smaller sized MIOPs (Fig. 1g) were almost uniform in shape while bigger-sized (Fig. 1a) reflected the most spherical shapes and had tendency to form big magnetite particles through the aggregation process. The comparison between smaller size (Fig. 1g) and bigger size (Fig. 1a) confirmed that, with decrease the flow of alkali addition, oxidation rate also has been decreased and the amount of the Fe with divalent has been increased (Thakur, 2009).

Result from Dynamic Light Scattering measurement and surface charged are presented in Fig. 2. There is a good match between flow rate of alkali addition and particle size. To illustrate the result, with decreased the flow rate of alkali addition, the particle size clearly has increased. In different range of particle size, the surface charged was same and positive charged directly related to treated condition with HNO₃. This behavior can be explained by a change in the type of formed stable complex. According to this effect

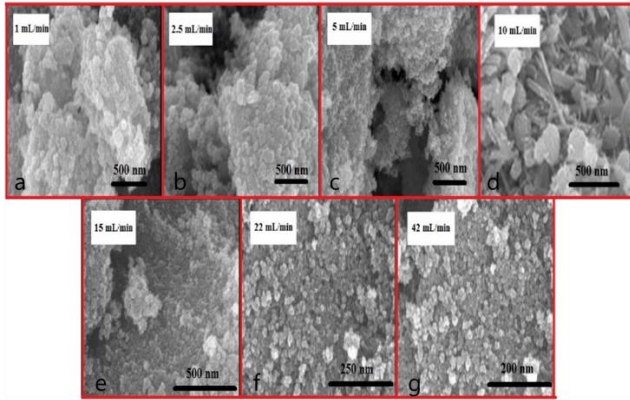


Fig. 1 The effect of varying alkali flow rate addition on the morphology of MIPOs in FESEM

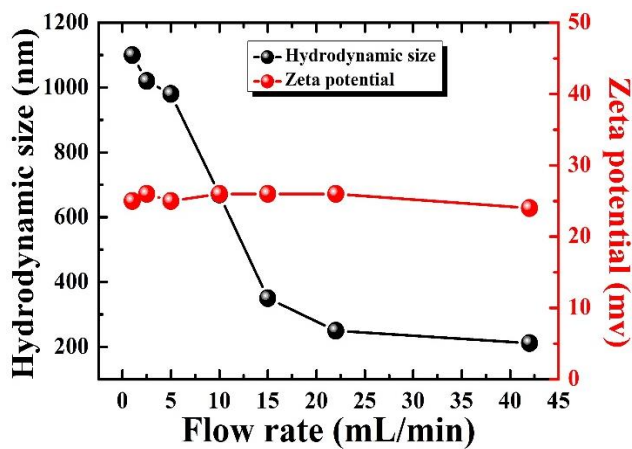


Fig. 2 The effect of varying alkali flowrate addition on the hydrodynamic size and net surface charge of MIPOs

indicates an increment of cation vacancy in the lattice, this behavior corroborated with the decreased value of the lattice parameter, which is shown in table below. These values are minor than the lattice parameter of defect free magnetite, this small reduction is assumed to be due to the prevalence of a small amount of cation deficiency +24 mv(Gupta, Bajpai and Bajpai, 2014).

The magnetization M_s of magnetite iron oxide particles were measured as a function of the applied magnetic field H with A 9600 VSM superconducting quantum interference device (S700X SQUID magnetometer). The hysteresis of the magnetization was obtained by changing H between +10,000 and -10,000 Oe. These measurements were carried out at 300 K as shown in Fig. 3.

The results indicated that these nanoparticles show supermagnetic behavior almost immeasurable coerciveness and remanance at room temperature. For smaller size, the amount of magnetization has been decreased significantly. The investigation show that this synthetic route presents a great result and good match as the average size of particles is getting smaller, the sample with the smallest diameter (200 nm) exhibits a saturation magnetization of 10 emu/g that is related to Fe⁺³ (oxidized form) γ -Fe₂O₃ maghemite. In bigger size (1130 nm) the amount magnetization increases dramatically to 60 emu/g.

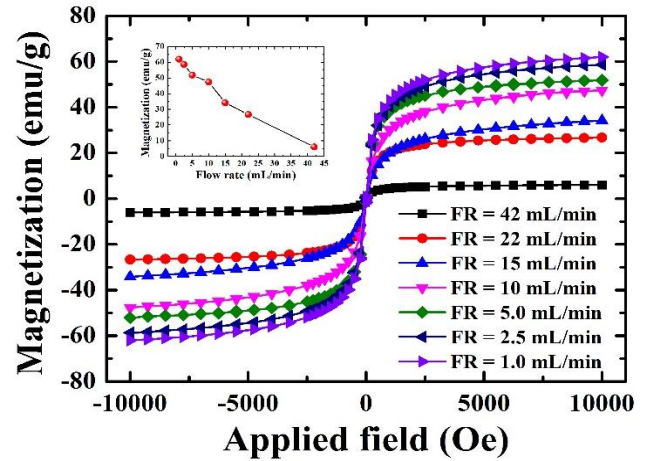


Fig. 3 The effect of varying alkali flowrate addition on the magnetization of MIPOs at different sizes.

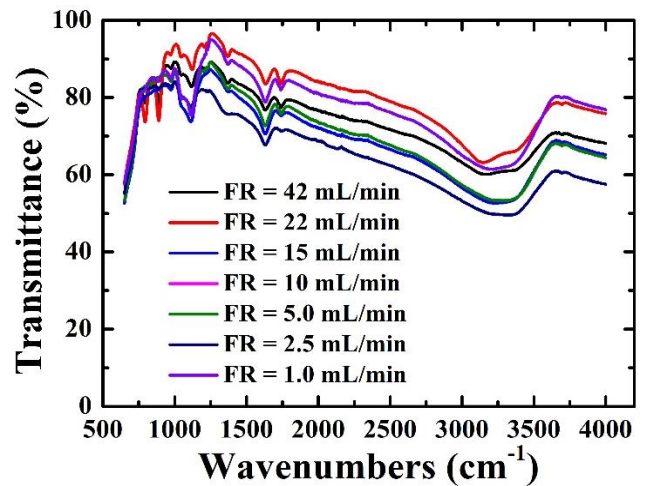


Fig. 4 Vibrational spectra of magnetic iron oxides of various sizes.

Figure 4 shows the FT-IR spectrum of different size of magnetite iron oxide. These results agree in good agreement with previous study by Sangeetha *et al.* In all spectrum clearly seen that, the peak at 1405 cm^{-1} is assigned the stretch bond of Fe-O of Fe₃O₄, which is characteristic band of magnetite. The broad band at 3413 cm^{-1} with moderate intensity is assigned to the presence of -OH group at the surface of MIPOs. During comparing different samples with each other, we can have concluded that, with decreasing the particle size, the percentage of transmission would be decrease.

3.2 Removal of BSA

Figure 5 shows the effect of MIPOs dose on BSA removal. With the increase of MIPOs dose BSA adsorption increase linearly up to 2.5 mg/L dose of MIPOs.

Whereas further increasing the dose of MIPOs have no substantial effect on the adsorption of BSA. To further explore the adsorption behavior of BSA, Freundlich and Langmuir isotherms were applied to the data set. The best

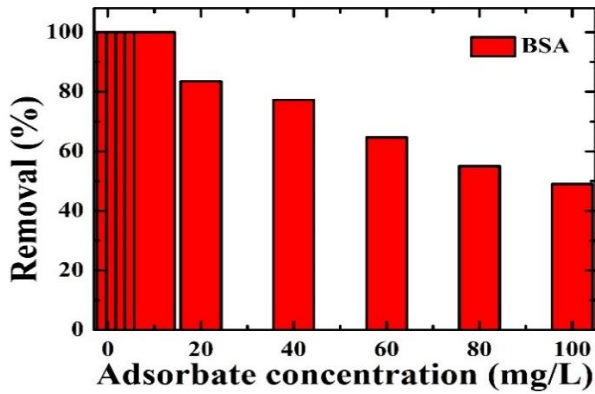


Fig. 5 Effect of different BSA concentrations on MIOPs removal capacity.

Table 2 Freundlich and Langmuir isotherms parameters for the BSA adsorption on MIOPs at room temperature

Isotherm	Parameters	MIOPs
Langmuir	R^2	0.901
	Q_{max} (mg/g)	64.7
	K_l (l/g)	0.49
Freundlich	R^2	0.778
	n	1.9
	K_f	21.1
	(mg/g (l/mg) ^{1/n})	

fit model was Langmuir isotherm with ($R^2=0.9$), which explain that MIOPs have maximum adsorption capacity Q_{max} of 64.7mg/g. For the complete removal of similar concentration of BSA the MIOPs dose required was 5g/L and 2.5mg/L, comparatively low dose of MIOPs was required to remove BSA from water. It may be because with in the similar concentration of BSA there is the difference in the molecular size and amount of molecules. For greater number of molecules here is the need of higher MIOPs dose because greater the molecules greater the negative charge and higher dose of MIOPs required to neutralize the charge.

Figure 6 shows the results of the average values for 4 runs and also the results of fitting the data by using Isotherm adsorption model was reported in Table 2 and shows the effect of different doses of MIOPs on the adsorption of BSA.

With the increase of MIOPs dose BSA adsorption increase with a linear trend up to 2.5 mg/L dose of MIOPs. To further explore the adsorption behavior of BSA, Freundlich and Langmuir isotherms were applied to the data set. However, Langmuir isotherm with ($R^2=0.9$), which explain that MIOPs have maximum adsorption capacity Q_{max} of 64.7mg/g. To further study the effect of BSA loading on MIOPs experiments were performed on the optimized dose 2.5mg/L of MIOPs. Different BSA loadings (2mg/L, 10mg/L, 20 mg/L, 60mg/L and 100mg/l) were selected and absorption behavior was studied with respect to time. It can be observed that BSA adsorption (mg/g) was decreased with the increase of BSA concentration. It can be the similar reason that for more amount of adsorbent more adsorbate is needed to neutralize the charge and shortage of

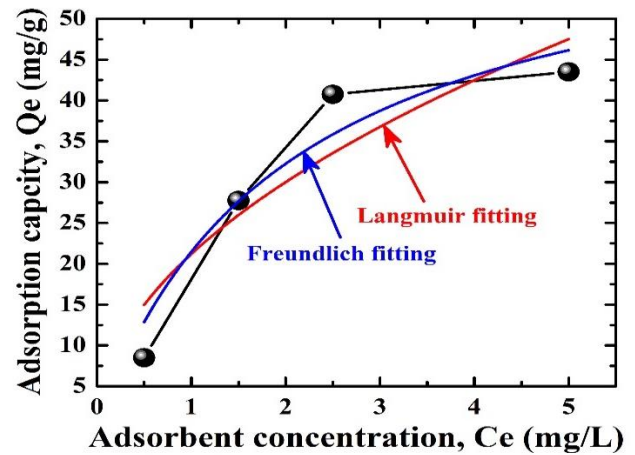


Fig. 6 Adsorption isotherm behavior of BSA on magnetic iron oxide particles.

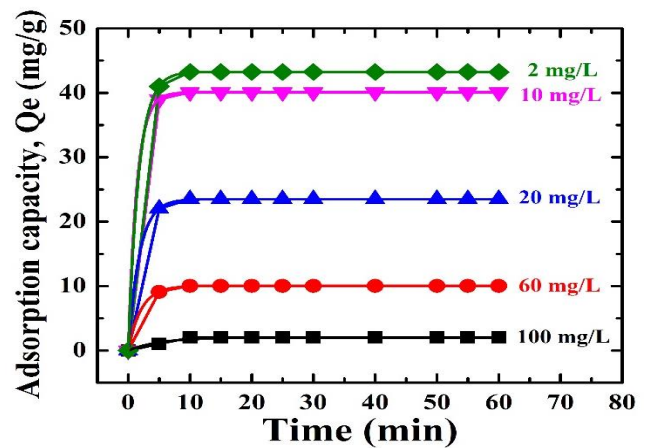


Fig. 7 Contact time of MIOPs on BSA adsorption at various BSA concentrations.

binding sites due to less adsorbent may also be the reason. Equilibrium was attained in first five minute for every concentration. This may be attributed to the larger size molecules of BSA which can easily be adsorbed. To further explain the kinetics of the BSA adsorption pseudo first and second order kinetics were applied to the dataset. However, pseudo first order model best fit to our experiments, it can be observed that adsorbed amount of BSA (Q_e) decrease dramatically with the increase of BSA concentration, as shown in Fig. 7.

3.3 Fouling mitigation

Figure 8 shows permeate flux and permeability of BSA-fouled membranes after cleaning. The smaller the size of the magnetic iron oxide, the higher is the surface area. Dead-end filtration experiments showed the higher adsorption of BSA on the smaller magnetic iron oxides resulting in relatively higher permeate flux. In a more practical sense if magnetic iron oxide would be used as adsorbents to reduce organic membrane fouling or at least delay the onset of the increase in the transmembrane pressure, the choice of the suitable particle size would greatly depend on the membrane pore size.

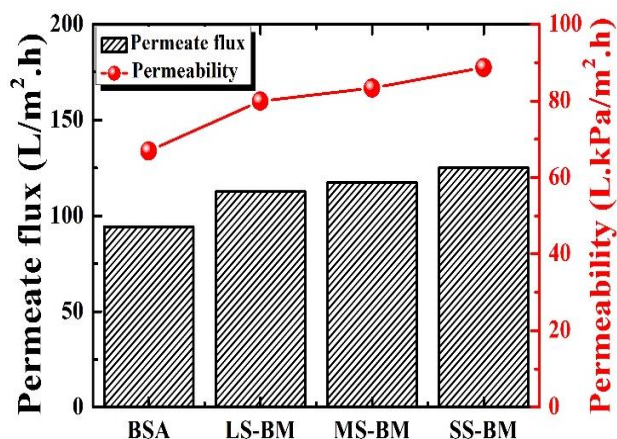


Fig. 8 Flux decline behaviour of BSA solution with different sized of magnetic iron oxide particles. LS-MB is referring to large size of MIOPs (1000 nm), MS-MB is middle size of MIOPs (680 nm) and SS-BM is the small size of MIOPs (210nm)

4. Conclusions

In this study magnetic iron oxide particles (MIOPs) were successfully synthesized by simple and low cost oven dried method. The particle size of MIOPs was controlled by regulating the flow rate of alkali addition. MIOPs particle size exhibited opposite trend with the alkali flow rate. The magnetization of MIOPs was significantly improved with increasing the flow rate. MIOPs with an efficient adsorption capacity for natural organic matter were employed for BSA protein model removal from water. The removal efficiency was increased to about 100% at lower concentrations of BSA protein. The effect of MIOPs adsorbent sizes on the absorption capacity of BSA was also studied. Permeate flux and water permeability of the BSA with the smallest size MIOPs membrane was increased during dead-end filtration. Our future work will be focused on the removal efficiency of other NOM such as HA from water with a comparative study as an extension of this article.

Acknowledgments

This study was supported by the Korea Ministry of the Environment (MOE) as “Technologies for the Risk Assessment and Management Program” (2017000140007).

References

Abbas, M., Tawfik, W. and Chen, J. (2018), “CdO nanorods and Cd(OH)₂/Ag core/satellite nanorods: Rapid and efficient sonochemical synthesis, characterization and their magnetic properties”, *Ultrasonics Sonochemistry*, **40**(August 2017), 577–582. <https://doi.org/10.1016/j.ultsonch.2017.08.002>.

Adegoke, H.I., Adekola, F.A., Fatoki, O.S. and Ximba, B.J. (2013), “Sorption interaction of oxyanions with iron oxides: A Review”, *Polish J. Environ. Studies*, **22**(1), 7–24.

Chen, K.L., Chen, J.H., Liao, S.H., Chieh, J.J., Horng, H.E., Wang, L.M. and Yang, H.C. (2015), “Magnetic clustering effect

during the association of biofunctionalized magnetic nanoparticles with biomarkers”, *PLoS ONE*, **10**(8), 1–12. <https://dx.doi.org/10.1371/journal.pone.0135290>.

Esmat, M., Farghali, A.A., Khedr, M.H. and El-Sherbiny, I.M. (2017), “Alginate-based nanocomposites for efficient removal of heavy metal ions”, *J. Biological Macromolecules*, **102**, 272–283. <https://doi.org/10.1016/j.jbiomac.2017.04.021>.

Gavrilescu, M. (2004), “Removal of heavy metals from the environment by biosorption”, *Eng. Life Sci.*, **4**(3), 219–232. <https://doi.org/10.1002/elsc.200420026>.

Gnanaprakash, G., Philip, J., Jayakumar, T. and Raj, B. (2007), “Effect of digestion time and alkali addition rate on physical properties of magnetite nanoparticles”, *J. Phys. Chem. B*, **111**(28), 7978–7986. <https://doi.org/10.1021/jp071299b>.

Guo, L., Du, Y., Yi, Q., Li, D., Cao, L. and Du, D. (2015), “Efficient removal of arsenic from “dirty acid” wastewater by using a novel immersed multi-start distributor for sulphide feeding”, *Separation Purification Technol.*, **142**, 209–214. <https://doi.org/10.1016/j.seppur.2014.12.029>.

Gupta, M.K., Bajpai, J. and Bajpai, A.K. (2014), “The biocompatibility and water uptake behavior of superparamagnetic poly(2-Hydroxyethyl methacrylate)-Magnetite nanocomposites as possible nanocarriers for magnetically mediated drug delivery system”, *J. Polym. Res.*, **21**(8), 518. <https://doi.org/10.1007/s10965-014-0518-0>.

Gutierrez, A.M., Dziubla, T.D. and Hilt, J.Z. (2017), “Recent advances on iron oxide magnetic nanoparticles as sorbents of organic pollutants in water and wastewater treatment”, *Reviews Environ. Health*, **32**(1–2), 111–117. <https://doi.org/10.1515/reveh-2016-0063>.

Hao, Y.M., Man, C. and Hu, Z.B. (2010), “Effective removal of Cu (II) ions from aqueous solution by amino-functionalized magnetic nanoparticles”, *J. Hazardous Mater.*, **184**(1–3), 392–399. <https://doi.org/10.1016/j.jhazmat.2010.08.048>.

Huang, Y. and Keller, A.A. (2015), “EDTA functionalized magnetic nanoparticle sorbents for cadmium and lead contaminated water treatment”, *Water Research*, **80**, 159–168. <https://doi.org/10.1016/j.watres.2015.05.011>.

Karaagac, O., Kockar, H., Beyaz, S. and Tanrisever, T. (2010), “A simple way to synthesize superparamagnetic iron oxide nanoparticles in air atmosphere: Iron ion concentration effect”, *IEEE Transactions Mag.*, **46**(12), 3978–3983. <https://doi.org/10.1109/TMAG.2010.2076824>.

Khalil, M.I. (2015), “Co-precipitation in aqueous solution synthesis of magnetite nanoparticles using iron(III) salts as precursors”, *Arabian J. Chem.*, **8**(2), 279–284. <https://doi.org/10.1016/j.arabjc.2015.02.008>.

Kim, K.J. and Jang, A. (2018), “Presence of Fe-Al binary oxide adsorbent cake layer in ceramic membrane filtration and their impact for removal of HA and BSA”, *Chemosphere*, **196**, 440–452. <https://doi.org/10.1016/j.chemosphere.2018.01.011>.

Lakouraj, M.M., Mojerlou, F. and Zare, E.N. (2014), “Nanogel and superparamagnetic nanocomposite based on sodium alginate for sorption of heavy metal ions”, *Carbohydrate Polym.*, **106**(1), 34–41. <https://doi.org/10.1016/j.carbpol.2014.01.092>.

Lee, N., Amy, G. and Lozier, J. (2005), “Understanding natural organic matter fouling in low-pressure membrane filtration”, *Desalination*, **178**(1–3, Special Issue), 85–93. <https://doi.org/10.1016/j.desal.2004.11.030>.

Li, M.Y. and Sui, X.D. (2012), “Synthesis and Characterization of Magnetite Particles by Co-Precipitation Method”, *Key Eng. Mater.*, **512–515**, 82–85. <https://doi.org/10.4028/www.scientific.net/KEM.512-515.82>.

Maher, A., Sadeghi, M. and Moheb, A. (2014), “Heavy metal elimination from drinking water using nanofiltration membrane technology and process optimization using response surface methodology”, *Desalination*, **352**, 166–173.

- <https://doi.org/10.1016/j.desal.2014.08.023>.
- Mascolo, M.C., Pei, Y. and Ring, T.A. (2013), "Room Temperature Co-Precipitation Synthesis of Magnetite Nanoparticles in a Large pH Window with Different Bases", *Mater.*, **6**(12), 5549–5567. <https://doi.org/10.3390/ma6125549>.
- Mehta, R.V. (2017), "Synthesis of magnetic nanoparticles and their dispersions with special reference to applications in biomedicine and biotechnology", *Mater. Sci. Eng. C*, **79**, 901–916. <https://doi.org/10.1016/j.msec.2017.05.135>.
- Semblante, G.U., Tampubolon, S.D.R., You, S.J., Lin, Y.F., Chang, T.C. and Yen, F.C. (2013), "Fouling reduction in membrane reactor through magnetic particles", *J. Membr. Sci.*, **435**, 62–70. <https://doi.org/10.1016/j.memsci.2013.02.003>.
- Tawfik, W.Z., Esmat, M. and El-Dek, S.I. (2017), "Drastic improvement in magnetization of CdO nanoparticles by Fe doping", *Appl. Nanosci.*, **7**(8), 863–870. <https://doi.org/10.1007/s13204-017-0623-6>.
- Thakur, S. (2009), "Nickel - Zinc ferrite from reverse micelle process: Structural and magnetic properties, mössbauer spectroscopy characterization", *J. Phys. Chem. C*. <https://doi.org/10.1021/jp9050287>.
- Tu, Y.J., You, C.F., Chang, C.K. and Wang, S.L. (2013), "XANES evidence of arsenate removal from water with magnetic ferrite", *J. Environ. Management*, **120**, 114–119. <https://doi.org/10.1016/j.jenvman.2013.02.006>.
- Wang, H., Ding, A., Gan, Z., Qu, F., Cheng, X., Bai, L., Guo, S., Li, G. and Liang, H. (2017), "Fluorescent natural organic matter responsible for ultrafiltration membrane fouling: Fate, contributions and fouling mechanisms", *Chemosphere*, **182**, 183–193. <https://doi.org/10.1016/j.chemosphere.2017.04.148>.
- Wang, J. and Chen, C. (2009), "Biosorbents for heavy metals removal and their future", *Biotechnol. Adv.*, **27**(2), 195–226. <https://doi.org/10.1016/j.biotechadv.2008.11.002>.
- Wang, L., Miao, R., Wang, X., Lv, Y., Meng, X., Yang, Y., Huang, D., Feng, L., Liu, Z. and Ju, K. (2013), "Fouling behavior of typical organic foulants in polyvinylidene fluoride ultrafiltration membranes: Characterization from microforces", *Environ. Sci. Technol.*, **47**(8), 3708–3714. <https://doi.org/10.1021/es4004119>.
- Xu, P., Zeng, G. M., Huang, D. L., Feng, C. L., Hu, S., Zhao, M. H., Lai, C., Wei, Z., Huang, C. Xin Xie, G. and Liu, Z.F. (2012), "Use of iron oxide nanomaterials in wastewater treatment: A review", *Sci. Total Environ.*, **424**, 1–10. <https://doi.org/10.1016/j.scitotenv.2012.02.023>.
- Zhang, S., Niu, H., Cai, Y., Zhao, X. and Shi, Y. (2010), "Arsenite and arsenate adsorption on coprecipitated bimetal oxide magnetic nanomaterials: MnFe₂O₄ and CoFe₂O₄", *Chem. Eng. J.*, **158**(3), 599–607. <https://doi.org/10.1016/j.cej.2010.02.013>